Turk J Phys
33 (2009) , 217 – 223.

doi:10.3906/fiz-0903-2

Thermoelectric power and low-field electron mobility in $Al_xGa_{1-x}N$ lattice-matched to GaN

H. ARABSHAHI
Department of Physics, Ferdowsi University of Mashhad,
P.O. Box 91775-1436, Mashhad-IRAN
e-mail: arabshahi@um.ac.ir

Received 03.03.2009

Abstract

The results of thermoelectric power and electron drift mobility in $Al_xGa_{1-x}N$ lattice-matched to GaN are calculated for different temperatures, free-electron concentrations and compositions. The two-mode nature of the polar optic phonons is considered jointly with deformation potential acoustic, piezoelectric, alloy and ionized-impurity scattering. Band non-parabolicity, admixture of p functions, arbitrary degeneracy of the electron distribution and the screening effects of free carriers on the scattering probabilities are incorporated. The Boltzmann equation is solved by an iterative technique using the currently established values of the material parameters. The iterative results are in fair agreement with other recent calculations obtained using the relaxation-time approximation and experimental methods.

Key Words: Thermoelectric power, optical phonon, piezoelectric, non-parabolicity, relaxation-time.

1. Introduction

III-nitride semiconductors have high prospects for applications in optical and electronic devices and have already been commercialized in applications such as light-emitting devices. III-nitrides are amenable to the advanced processes necessary for achieving thermoelectric devices such as independent power supplies for low electric power devices [1–2]. As an aid to the device-related work, the transport coefficients of the material need careful investigation. Electron mobility in the ternary alloy has been measured, Monte Carlo calculations of mobility have also been performed [3]. In the mean time our knowledge of the basic parameters and of the scattering mechanisms for the alloy has improved. Particularly, it is now known that the polar-phonon scattering, which is the dominant lattice scattering mechanism in the ternary alloy, has a two-mode character [4]. It is important to calculate the transport coefficients using such currently available information on scattering mechanisms and material parameters. We use such information in the present paper to calculate electron

mobility and thermoelectric power in the $Al_xGa_{1-x}N$ alloy. We consider band non-parabolicity, admixture of p-type valence-band wave functions, degeneracy of the electron distribution to any arbitrary degree and the screening effects of free carriers on the scattering probabilities. Electrons in bulk material suffer intravalley scattering by polar optical, non-polar optical, alloy and acoustic phonons, and piezoelectric scattering and ionized impurity scattering. Acoustic and piezoelectric scattering are assumed elastic and the absorption and emission rates are combined under the equipartition approximation which is valid for lattice temperatures above 77 K. Elastic ionized impurity scattering is described using the screened Coulomb potential of the Brooks-Herring model [5–8]. The Boltzmann equation is solved iteratively for our purpose jointly incorporating the effects of all the scattering mechanisms. Our calculated results are compared with the available experimental data on both the temperature and the composition dependence of mobility.

This paper is organized as follows. Details of the iterative model and the electron mobility and thermoelectric power calculations are presented in section 2 and the results of iterative calculations carried out on $Al_xGa_{1-x}N$ structures are interpreted in section 3.

2. Theoretical model

In principle the iterative technique gives exact numerical prediction of electron mobility in bulk semiconductors. To calculate mobility, we solve the Boltzmann equation to get the modified probability distribution function under the action of a steady electric field. Here, we have adopted the iterative technique for solving the Boltzmann transport equation. The electron distribution function $f(k)$ in the presence of an electric field E is expressed as

$$f(k) = f_0(k) + \left[\frac{e\hbar E}{m^*}\right] k f_1(k) \times (\partial f_0/\partial E)\cos\theta \tag{1}$$

where $f_0(E)$ is the thermal equilibrium Fermi-Dirac distribution function, e is the magnitude of the electron charge, θ is the angle between k and E and $f_1(k)$ is the perturbation function to be determined from the Boltzmann equation. The Boltzmann equation for electrons with Fermi-Dirac statistics describes classical transport phenomena with which we are presently concerned exclusively. Allowing for an electric field E and a spatial gradient parallel to E, we have [9–10]

$$v \cdot \nabla f_T + \frac{e}{\hbar} E \cdot \nabla_k f_k = \int [s' f'_T(1 - f_T) - s f_T(1 - f'_T)]\, dk' \tag{2}$$

where $f'_T = f_T(k')$, $s = s(k, k')$ and $s' = s(k', k)$ is the differential scattering rate for an electron in the state characterized by k' to make a transition into the state characterized by k.

Consider electrons in an isotropic, non-parabolic conduction band whose equilibrium Fermi distribution function is $f_0(k)$ in the absence of electric field. Note the equilibrium distribution $f_0(k)$ is isotropic in k space but is perturbed when an electric field is applied. If the electric field is small, we can treat the change from the equilibrium distribution function as a perturbation which is first order in the electric field. The distribution in the presence of a sufficiently small field can be written quite generally as

$$f(k) = f_0(k) + f_1(k)\cos\theta \tag{3}$$

where θ is the angle between k and E and $f_1(k)$ is an isotropic function of k, which is proportional to the magnitude of the electric field. $f(k)$ satisfies the Boltzmann equation 2 and it follows that

$$\frac{eE\cos\theta}{\hbar}\frac{\partial f_0}{\partial k} = \sum_i \left\{ \int \cos\theta' f_1'[s_i'(1-f_0) + s_i f_0]d^3k' - f_1 \cos\theta \int [s_i(1-f_0') + s_i' f_0']d^3k' \right\} \tag{4}$$

where the sum is over scattering processes i. For a more compact notation we have written $f(k')=f'$, $s_i(k,k')=s_i$ and $s_i(k',k)=s_i'$. $s_i(k,k')=s_i$ is the probability for scattering out of state k into the differential element d^3k' at k'. For the isotropic conduction band $s_i(k,k')$ depends on only k, k' and the cosine of angle ϕ between them, and the relation

$$\int \cos\theta' A(\cos\phi)d^3k' = \cos\theta \int \cos\phi A(\cos\phi)d^3k' \tag{5}$$

may be used to manipulate equation 4. Here, $A(\cos\phi)$ is an arbitrary function of $\cos\phi$ but does not otherwise depend on θ and θ'.

From equation 4 and 5 we obtain

$$\frac{eE}{\hbar}\frac{\partial f_0}{\partial k} = \sum_i \left\{ \int \cos\phi f_1'[s_i'(1-f_0) + s_i f_0]d^3k' - f_1 \int [s_i(1-f_0') + s_i' f_0']d^3k' \right\}. \tag{6}$$

In general there will be both elastic and inelastic scattering. For example, impurity scattering is elastic and acoustic and piezoelectric scattering are elastic to a good approximation at room temperature. However, polar and non-polar optical phonon scattering are inelastic. Several authors have calculated the electron scattering rates [11–13]. Labeling the elastic and inelastic scattering rates with subscripts el and iel, respectively, and recognizing that, for any process i, $s_{\mathrm{el}i}(k',k)=s_{\mathrm{el}i}(k,k')$, equation 6 can be written as

$$f_1(k) = \frac{(-eE/\hbar)(\partial f_0/\partial k) + \sum_j \int \cos\phi f_1'[s_{\mathrm{iel}j}'(1-f_0) + s_{\mathrm{iel}j} f_0]d^3k'}{\sum_i \int (1-\cos\phi)s_{\mathrm{el}i}d^3k' + \sum_j \int [s_{\mathrm{iel}j}(1-f_0') + s_{\mathrm{iel}j}' f_0']d^3k'}. \tag{7}$$

Note the first term in the denominator is simply the momentum relaxation rate for elastic scattering. Equation 7 may be solved iteratively by the relation

$$f_{1n}(k) = \frac{(-eE/\hbar)(\partial f_0/\partial k) + \sum_j \int \cos\phi f_1(k')[n-1][s_{\mathrm{iel}j}'(1-f_0) + s_{\mathrm{iel}j} f_0]d^3k'}{\sum_i \int (1-\cos\phi)s_{\mathrm{el}i}d^3k' + \sum_j \int [s_{\mathrm{iel}j}(1-f_0') + s_{\mathrm{iel}j}' f_0']d^3k'}, \tag{8}$$

where $f_{1n}(k)$ is the perturbation to the distribution function after the n^{th} iteration. It is interesting to note that if the initial distribution is chosen to be the equilibrium distribution, for which $f_1(k)$ is equal to zero, we get the relaxation time approximation result after the first iteration. We have found that convergence can normally be achieved after only a few iterations for small electric fields. Once $f_1(k)$ has been evaluated to the required accuracy, it is possible to calculate quantities such as the drift mobility μ, which is given by

$$\mu = \frac{\hbar}{3m^*E}\frac{\int_0^\infty (k^3/1+2\alpha E')\phi dk}{\int_0^\infty k^2 f_0 dk}. \tag{9}$$

The thermoelectric power Q is the ratio of electric field E to temperature gradient ∇T across an open-circuited crystal, i.e., the electron current density J is set equal to zero. Theoretically, the current density in the presence of electric field E and temperature gradient ∇T in an isotropic crystal is

$$J = \sigma \left[E - (\nabla E_{\mathrm{F}}/e) - Q\nabla T \right], \tag{10}$$

where σ is the conductivity and E_{F} is the Fermi energy.

Equation 10 is valid for the small driving forces considered here for which σ and Q are independent of the field strengths. When J=0, as in the open-circuit measurement of Q, the crystal maintains equilibrium so that ∇E_{F}=0 and

$$Q = E/(\partial T/\partial z), \tag{11}$$

which is the defining equation for Q. The temperature gradient is taken parallel to the z axis. Since all driving forces are small, the transport coefficients σ and Q are constant and equation 11 yields Q also in the short-circuit case when E=0

$$Q = -\left[\frac{\partial E_{\mathrm{F}}}{\partial z}/e + \frac{J}{\sigma} \right] / \frac{\partial T}{\partial z}. \tag{12}$$

Substitution Poisson's equation and Fermi-Dirac distribution function in equation 12, the thermoelectric power is

$$Q = \frac{k}{e} \left[\frac{\int k^2 f(1-f)(E/T)dk}{\int k^2 f(1-f)dk} - \frac{E_{\mathrm{F}}}{kT} \right] - \frac{J/\sigma}{\partial T/\partial z}. \tag{13}$$

Important parameters used throughout the simulations are listed in Table 1.

Table 1. Material parameter selections for wurtzite GaN and $Al_{0.2}Ga_{0.8}N$ [3–8].

Bulk material parameters	GaN	$Al_{0.2}Ga_{0.8}N$	
Density ρ(kgm^{-3})	6150	3814	
Lattice constant a_0 (Å)	3.139	3.12	
Polar optical phonon energy $\hbar\omega_{po}$ (eV)	0.0995	0.0992	
Longitudinal sound velocity v_s(ms^{-1})	4330	4522	
Low-frequency dielectric constant ϵ_s	9.5	8.7	
High-frequency dielectric constant ϵ_∞	5.35	4.88	
Valley dependent parameters	Γ	U	K
GaN:			
Effective mass (m*/m$_0$)	0.18	0.4	0.3
Nonparabolicity (eV^{-1})	0.189	0.065	0.7
$Al_{0.2}Ga_{0.8}N$:			
Effective mass (m*/m$_0$)	0.28	0.35	0.49
Nonparabolicity (eV^{-1})	0.29	0.41	0.16

3. Calculation results

Figure 1 shows the temperature dependence of electron drift mobility in $Al_xGa_{1-x}N$ for x=0.2, 0.4 and 0.5. In curve 1, the carrier concentration is taken to be n=10^{17} cm^{-3}. The ionized impurity concentration is put equal to the electron concentration. In curve 2, n is taken to be n=5×10^{17} cm^{-3} and in curve 3, n is given the value of 10^{18} cm^{-3}. It can be observed that the mobility of electrons decrease with increasing temperature because of increasing optical phonon scattering rate. Also, it is seen that with increasing composition from 0.2 to 0.5 the calculated electron mobility is decreased because of a higher impurity scattering rate.

Figure 2 shows the mobility of electrons versus composition for various doping concentration. The difference can be understood by considering difference in the electric parameters of the materials like electron effective mass in the central Γ valley.

The temperature variation of thermoelectric power Q for x=0.2 is shown in Figure 3. The magnitude of Q increases with temperature mainly because the material becomes more nondegenerate with a rise in temperature. Also, assuming that the material is uncompensated, the thermoelectric power for n=10^{18} (curve 3) is larger in magnitude than for n=10^{17} (curve 1) since the Fermi level is higher in the latter case. Considering curves 1 and 3, we find that the magnitude of Q for a compensated sample is larger. This is due to the enhancement of ionized impurity scattering.

The room temperature values of Q for an uncompensated material are plotted as a function of x in Figure 4. The effective mass decreases with x, causing an upward movement of the Fermi level with a rise in x. This results in the decrease of Q with increasing x. It is clear from Figure 4 that inclusion of ionized impurity scattering enhances Q while that of alloy scattering reduces Q. Our calculated results on thermoelectric power could not be compared with experiments since no such data could be traced in the literature.

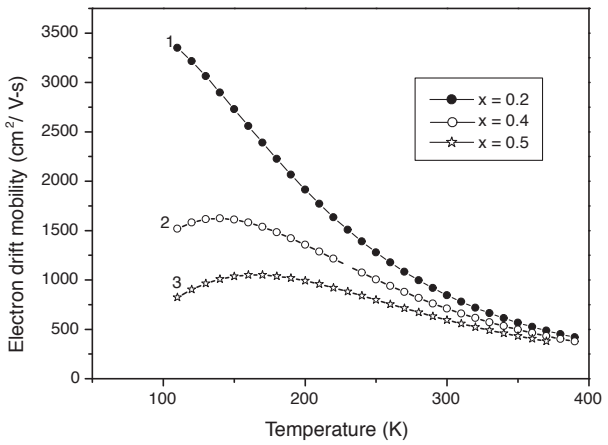

Figure 1. Variation of electron drift mobility with temperature for $Al_xGa_{1-x}N$ lattice-matched to GaN, for x=0.2 (curve 1), x=0.4 (curve 2) and x=0.5 (curve 3). In curve 1, n=10^{17} cm^{-3}; in curve 2, n=5×10^{17} cm^{-3}; and in curve 3, n=10^{18} cm^{-3}.

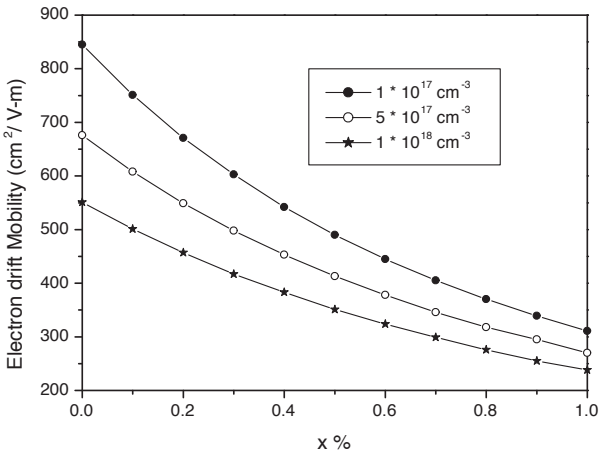

Figure 2. Variation of electron drift mobility with composition for $Al_xGa_{1-x}N$ lattice-matched to GaN at room temperature. Calculated curves are for n=10^{17}, 5×10^{17} and n=10^{18} cm^{-3}.

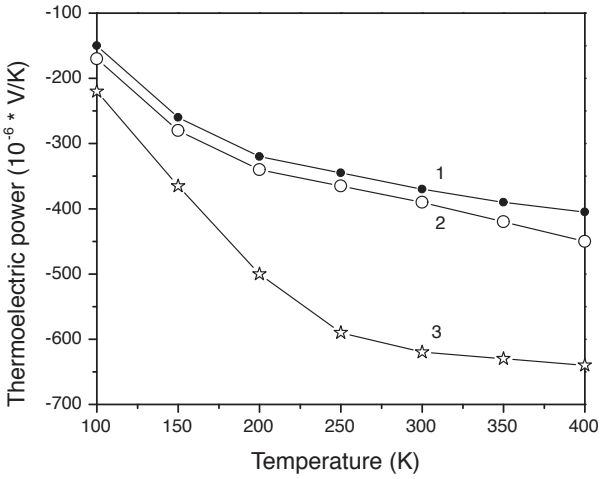

Figure 3. Temperature dependence of thermoelectric power of $Al_xGa_{1-x}N$ lattice-matched to GaN for x=0.2. In curve 1, n=10^{17}, in curve 2, n=5×10^{17} and in curve 3, n=10^{18} cm^{-3}.

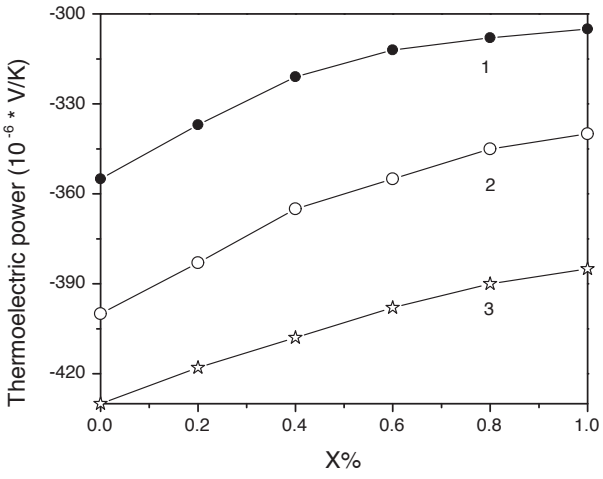

Figure 4. Composition (x) dependence of room temperature values of thermoelectric power of $Al_xGa_{1-x}N$ lattice-matched to GaN. In curve 1, n=10^{17}, in curve 2, n=5×10^{17} and in curve 3, n=10^{18} cm^{-3}.

4. Conclusions

Electron mobility and thermoelectric power of $Al_xGa_{1-x}N$ lattice-matched to GaN by an iterative solution of the Boltzmann equation have been carried out. The details of band structure and scattering mechanisms are included without applying Matthiessen's rule. Our results show that the experimental values of mobility can be explained with a lower degree of compensation than indicated by some previous simple analysis.

Acknowledgments

I would like to thank for partial supports of this work by Ferdowsi University of Mashhad.

References

[1] U. V. Bhapkar and M. Shur, *Appl. Phys. Lett.*, **82**, (1997), 1649.

[2] B. E. Foutz, L. F. Eastman, U. V. Bhapkar and M. Shur, *Appl. Phys. Lett.*, **70**, (1997), 2849

[3] E. Bellotti, B. K. Doshi and K. F. Brennan, *J. Appl. Phys.*, **85**, 916 (1999)

[4] M. Frahmand, *IEEE Transaction on Electron Devices*, **48** 535 (2001)

[5] K. Brennan, K. Hess and J. Tang, *IEEE Trans. Electron Devices*, **30**, (1983), 1750.

[6] H. Arabshahi, *Modern Physics Letters B.*, **21**, (2007), 199.

[7] H. Arabshahi, M. Rezaee and M. Dastras, *Modern Physics Letters B.*, **28**, (2008), 2793.

[8] M. Rezaee, H. Arabshahi and M. Benam, *Modern Physics Letters B.*, **28**, (2008), 1357.

[9] C. Moglestue, *Monte Carlo Simulation of Semiconductor Devices*, (Chapman and Hall. 1993) p.120.

[10] C. Jacoboni and P. Lugli, *The Monte Carlo Method for semiconductor and Device Simulation*, (Springer-Verlag. 1989) p.87.

[11] J. Kolnik, I. H. Oguzman and K. F. Brennan, *J. Appl. Phys.*, **81**, (1997), 726.

[12] M. A. Littlejohn, J. R. Hauser and T. H. Glisson, *Appl. Phys. Lett.*, **83**, (1975), 625.

[13] K. F. Brennan, D. H. Park, K. Hess and M. A. Littlejohn, *J. Appl. Phys.*, **63**, (1988), 5004.